PHYSICS AND CHEMISTRY OF SOLID STATE
V. 27, No. 3 (2026) pp. 525-531
Section: Physics

DOI: 10.15330/pcss.27.3.525-531

Vasyl Stefanyk Carpathian National University

ФІЗИКА І ХІМІЯ ТВЕРДОГО ТІЛА
Т. 27, № 3 (2026) С. 525-531
Фізико-математичні науки

PACS: 73.21.La

ISSN 1729-4428 (Print)
ISSN 2309-8589 (Online)

R.Ya. Leshko[1], O.V. Leshko[1], I.V. Bilynskyi[1,2], Ya.Yu. Melnyk[2], A.O. Ocheretyanyi[2], O.I. Chekin[2], M.V. Kvyk[2]

Electron energy spectrum of separated and fused spherical quantum dots

[1]*Department of physics and information systems, Drohobych Ivan Franko State Pedagogical University, Drohobych, Ukraine, leshkoroman@dspu.edu.ua;*
[2]*Department of physics, Kryvyi Rih State Pedagogical University, Kryvyi Rih, Ukraine*

We present a highly efficient semi-analytical approach to model electronic states in fused spherical quantum dots by deriving an exact analytical Fourier transform of their 3D shape function using cylindrical Bessel functions. This mathematical novelty allows the direct application of the plane-wave expansion method to solve the Schrödinger equation with a spatially dependent effective mass, completely eliminating the need for resource-intensive 3D spatial meshing. Applying this to a GaAs/AlGaAs heterostructure, we demonstrate that strong geometric overlap induces robust quantum-mechanical hybridization, causing an exponential splitting of degenerate energy levels into symmetric and antisymmetric states. The model guarantees an exact asymptotic transition to isolated quantum dot solutions, providing a fast and rigorous tool for prototyping complex nanostructures.

Keywords: fused and coupled quantum dots, electron energy spectrum, wave function hybridization.

Received 12 March 2026; Accepted 02 September 2026; Published 18 September 2026.

Introduction

Semiconductor nanocrystals, or quantum dots (QDs), are among the most intensively studied objects in modern solid-state physics and nanotechnology [1-3]. Due to the three-dimensional spatial confinement of charge carriers, their electronic and optical properties differ significantly from those of bulk materials and can be flexibly controlled by varying the nanoparticle dimensions. This makes QDs ideal candidates for application in a wide range of modern devices, including next-generation lasers, light-emitting diodes, solar cells, biosensors, and as building blocks for quantum information technologies [4-7].

The rapid development of synthesis technologies has enabled the creation of nanostructures with an unprecedented level of control over their parameters. To date, there are various methods for obtaining QDs, among which molecular beam epitaxy and colloidal chemical synthesis take the leading roles [8-9]. Thanks to the refinement of these techniques, it is possible to grow nanocrystals of various geometric shapes: spherical, cubic, pyramidal, conical, as well as structures with complex topologies, such as quantum rings or nanostars [10-14]. Such a diversity of shapes and sizes opens up broad possibilities for the fine engineering of the energy spectrum and charge carrier wave functions.

Of particular practical interest is the colloidal synthesis method, which is technologically accessible and allows for the production of large arrays of nanoparticles in solutions. However, during the formation of closely packed films or superlattices, especially upon the removal of stabilizing surface ligands, colloidal QDs often undergo agglomeration and fusion [2, 3, 15-18]. Experimental studies and atomistic modeling show that two separate QDs can efficiently merge through direct surface attachment (oriented attachment), forming a single structure–the so-called fused QD or artificial molecule [3, 17]. This process is accompanied by a rearrangement of the crystal lattice in the contact region and the formation of a shared electronic system. Similar to the formation of

covalent bonds in real molecules, the fusion of nanocrystals leads to strong quantum coupling, wave function hybridization, and the splitting of energy levels into bonding and antibonding states [2]. Furthermore, the ordered epitaxial fusion of nanocrystals is currently considered one of the most promising pathways for creating two-dimensional and three-dimensional superlattices with unique charge transport properties [15].

Theoretical investigation of the energy spectrum of complex-shaped and coupled nanostructures is important for understanding and predicting their physical properties. The electronic states in isolated QDs of various symmetries have been studied in detail in the literature [19-21]. Significant attention is also traditionally devoted to systems of two or more QDs [22] that are separated by a physical potential barrier (e.g., a matrix layer) and interact exclusively through quantum-mechanical tunneling. However, systems of fused QDs (in which the geometric barrier between nanocrystals completely disappears and charge carriers move freely within a combined quantization region of a complex shape) require a separate theoretical approach. Certain aspects of the electronic structure of fused QDs have been investigated using density functional theory and pseudopotentials [18], but the detailed and continuous evolution of the spectrum during the geometric transition from two isolated spheres to a single combined structure requires further systematic study.

In this work, we investigate the electron energy spectrum of a system of two spherical quantum dots, comparing the regimes of isolated nanocrystals and the structure formed as a result of their fusion. The main objective is to analyze the evolution of the energy levels and electron wave functions depending on the degree of geometric overlap (the distance between the centers) of the QDs, as well as to construct an analytical theory to describe such systems.

I. Heterosystem model

We consider the QD formed by the intersection of two identical spheres of radius a, separated by an inter-center distance D (fig. 1). The electron effective mass inside the QD is denoted by m_0, while the QD itself is embedded in a matrix characterized

To mathematically describe this complex geometry, it is convenient to place the origin of the Cartesian coordinate system exactly in the middle between the centers of the spheres on the z-axis. Thus, the coordinates of the centers are $\vec{r}_1 = (0, 0, -D/2)$ and $\vec{r}_2 = (0, 0, D/2)$. The three-dimensional geometric boundary of the fused QD can be entirely defined by a single analytical shape function r, which equals to unity inside the quantization region and zero outside:

$$f(\vec{r}) = \begin{cases} 1, & \text{in QD,} \\ 0, & \text{otherwise.} \end{cases} \quad (1)$$

Using this shape function, the spatial distribution of the confinement potential $U(\vec{r})$ and the position-dependent electron effective mass $m(\vec{r})$ for the entire heterostructure can be expressed in a compact form:

$$U(\vec{r}) = U_0[1 - f(\vec{r})], \quad (2)$$

$$\frac{1}{m(\vec{r})} = \frac{1}{m_1} + \left(\frac{1}{m_0} - \frac{1}{m_1}\right) f(\vec{r}), \quad (3)$$

where U_0 is the height of the potential barrier in the host matrix.

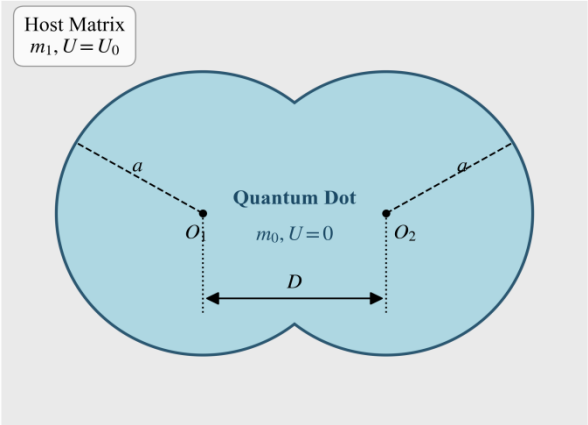

Fig. 1. Schematic cross-section of the modeled QD formed by two intersecting identical spheres of radius a. The distance between the centers of the spheres (O_1 and O_2) is denoted by D.

Since the effective electron mass inside the fused QD differs from the mass in the surrounding host matrix, we must employ the Hermitian kinetic energy operator in the Ben-Daniel-Duke form. The stationary Schrödinger equation for the electron is given by:

$$\hat{H}\psi(\vec{r}) = \left[-\frac{\hbar^2}{2}\vec{\nabla}\cdot\left(\frac{1}{m(\vec{r})}\vec{\nabla}\right) + U(\vec{r})\right]\psi(\vec{r}) = E\psi(\vec{r}) \quad (4)$$

To apply the plane wave expansion method (PWEM), we embed the nanostructure into an artificial rectangular supercell of volume $V = L_x L_y L_z = L^3$. The dimensions of the supercell are chosen to be sufficiently large so that the wave function decays to zero at its boundaries, thus eliminating the interaction between adjacent supercells. The value L has been used the same like in works [23-25]. We expand the electron wave function in a series over an orthonormal basis of plane waves:

$$\psi(\vec{r}) = \frac{1}{\sqrt{V}}\sum_{\vec{k}} c_{\vec{k}}\, e^{i\vec{k}\cdot\vec{r}}. \quad (5)$$

where $\vec{k}$ is the wave vector whose components take discrete values $k_i = 2\pi n_i/L$ ($i = x, y, z$; $n_i \in Z$), and $\boldsymbol{c}_{\vec{k}}$ are the unknown expansion coefficients.

Substituting this expansion into the Schrödinger equation (4) and multiplying from the left by $1/\sqrt{V}\, e^{-i\vec{k}\cdot\vec{r}}$, after integrating over the supercell volume, we obtain a standard algebraic eigenvalue problem:

$$\sum_{\vec{k}} H_{\vec{k}',\vec{k}}\, c_{\vec{k}} = E c_{\vec{k}'}. \quad (6)$$

The Hamiltonian matrix elements can be calculated analytically. Let us denote the difference vector as $\vec{q} = \vec{k}' - \vec{k}$. By applying the divergence theorem to the

kinetic energy operator, the matrix element takes the form:

$$H_{\vec{k}',\vec{k}} = \frac{\hbar^2}{2}(\vec{k}' \cdot \vec{k})M(\vec{q}) + U(\vec{q}), \quad (7)$$

where $M(\vec{q})$ and $U(\vec{q})$ are the Fourier transforms of the inverse effective mass and the potential respectively:

$$M(\vec{q}) = \frac{1}{V}\int_V \frac{1}{m(\vec{r})} e^{-i\vec{q}\cdot\vec{r}} d^3r = \frac{1}{m_1}\delta_{\vec{q},0} + \left(\frac{1}{m_0} - \frac{1}{m_1}\right) f(\vec{q}), \quad (8)$$

$$U(\vec{q}) = \frac{1}{V}\int_V U(\vec{r}) e^{-i\vec{q}\cdot\vec{r}} d^3r = U_0\delta_{\vec{q},0} - U_0 f(\vec{q}). \quad (9)$$

Here, $\delta_{\vec{q},0}$ is the Kronecker delta, and $f(\vec{q})$ is the Fourier transform of the fused QD shape function. Substituting these expressions yields the final compact formula for the Hamiltonian matrix elements:

$$H_{\vec{k}',\vec{k}} = \left[\frac{\hbar^2|\vec{k}|^2}{2m_1} + U_0\right]\delta_{\vec{k}',\vec{k}} + \left[\frac{\hbar^2}{2}\left(\frac{1}{m_0} - \frac{1}{m_1}\right)(\vec{k}' \cdot \vec{k}) - U_0\right] f(\vec{k}' - \vec{k}). \quad (10)$$

The next tack lies in determining the function and $f(\vec{q})$. Since the quantization region is the union of two intersecting spheres, the volume integral cannot be simply reduced to the sum of two independent spheres due to the double counting of the intersection region (the "lens"). We apply the inclusion-exclusion principle:

$$f(\vec{r}) = f_1(\vec{r}) + f_2(\vec{r}) - f_{inter}(\vec{r}), \quad (11)$$

where f_1 and f_2 are the shape functions of the isolated spheres with centers at (0, 0, -*D*/2) and (0, 0, *D*/2), and f_{inter} is the shape function of their intersection region. Due to the linearity of the Fourier transform, we have:

$$f(\vec{q}) = f_1(\vec{q}) + f_2(\vec{q}) - f_{inter}(\vec{q}). \quad (12)$$

The Fourier transform of a single sphere of radius *a*, shifted by a vector $\vec{r}_0$, is analytically known (like in [23-26]):

$$S(\vec{q}, \vec{r}_0) = e^{-i\vec{q}\cdot\vec{r}_0}\frac{4\pi}{Vq^3}\left(\sin(qa) - qa\cos(qa)\right). \quad (13)$$

Thus, the sum of the two spheres yields:

$$f_1(\vec{q}) + f_2(\vec{q}) = S(\vec{q}, 0)\left(e^{iq_zD/2} + e^{-iq_zD/2}\right) = 2\cos\left(\frac{q_zD}{2}\right)\cdot\frac{4\pi}{Vq^3}\cdot\left(\sin(qa) - qa\cos(qa)\right). \quad (14)$$

To calculate f_{inter}, we switch to a cylindrical coordinate system (ρ, ϕ, z). The intersection region is bounded along the *z*-axis from -*h* to *h*, where $h = a - D/2$. The cross-sectional radius at height z is given by $\rho_{max}(z) = \sqrt{a^2 - (|z| + D/2)^2}$.

Expressing the vector $\vec{q}$ in cylindrical coordinates as $\vec{q} = (q_{\|}\cos\phi_q, q_{\|}\sin\phi_q, q_z)$, where $q_{\|} = \sqrt{q_x^2 + q_y^2}$, $\phi_q = \arctan(q_y, q_x)$ the integral takes the form:

$$f_{inter}(\vec{q}) = \frac{1}{V}\int_{-h}^{h} dz\, e^{-iq_zz}\int_0^{\rho_{max}(z)} \rho\, d\rho \int_0^{2\pi} d\phi e^{-iq_{\|}\rho\cos(\phi - \phi_q)}. \quad (15)$$

Integration over the angle ϕ yields the zeroth-order Bessel function of the first kind, $2\pi J_0(q_{\|}\rho)$. The subsequent integration over ρ utilizes the standard property of Bessel functions $\int xJ_0(x)dx = xJ_1(x)$. As a result, we obtain a single one-dimensional integral:

$$f_{inter}(\vec{q}) = \frac{2\pi}{Vq_{\|}}\int_{-(a-D/2)}^{a-D/2} \rho_{max}(z) J_1\left(q_{\|}\rho_{max}(z)\right) e^{-iq_zz} dz. \quad (16)$$

This integral f_{inter} quantitatively describes the geometric overlap correction. For the case of separated quantum dots ($D > 2a$), the intersection region vanishes, $h = 0$, and consequently $f_{inter} = 0$.

Using the derived analytical expressions, we investigated the dependence of the electron energy spectrum in the fused QD on its geometric parameters.

II. Analysis of the obtained results

The numerical calculations were performed for a model system based on the GaAs/$Al_xGa_{1-x}As$ heterostructure. This material system serves as an excellent physical prototype for our calculations, as it allows for the formation of complex quantum nanostructures, including coalesced and fused quantum dots, which are often synthesized via droplet epitaxy [27,

28]. For the calculations, we adopted the standard parameters for an Al concentration of $x = 0.3$ [3]. The electron effective mass inside the GaAs QDs is $m_0 = 0.067\ m_e$, while in the $Al_xGa_{1-x}As$ host matrix it is $m_1 = 0.092\ m_e$. The finite potential barrier for electrons at the interface, determined by the conduction band offset, is relatively small $U_0 = 0.26$ eV). This relatively low barrier height physically justifies the application of the plane-wave expansion method and ensures its fast computational convergence.

Figure 2 presents the calculated dependencies of the ground E_0 and the first excited E_1 electron state energies on the inter-center distance D for four different sphere radii. The analysis of these curves reveals several physical features of the energy spectrum evolution during the fusion process. First, a general trend of decreasing energy for all levels is observed as the distance D is reduced. This is a direct consequence of the quantum confinement effect: as the spheres approach and intersect, the effective volume of the quantization region expands, leading to a reduction in the kinetic energy of the localized electron. Naturally, for smaller QDs (panel A, $a = 3$ nm), the spatial confinement is stronger, resulting in significantly higher absolute energy values compared to larger dots (panel D, $a = 6$ nm). Second, in the regime of strong geometric overlap ($D < 2a$), the effect of quantum mechanical coupling becomes pronounced, analogous to the formation of a covalent bond in diatomic molecules. Due to the hybridization of the electron wave functions of the two constituent spheres, the initially degenerate energy levels split into a symmetric ground state (bonding state, E_0) and an antisymmetric first excited state (antibonding state, E_1). The magnitude of this energy splitting, $\Delta E = E_1 - E_0$, monotonically increases as D decreases. This enhancement is attributed to the expansion of the cross-sectional area of the "neck" connecting the two spheres, which facilitates strong wave function delocalization and inter-dot electronic coupling.

To verify the theoretical model, the energy spectrum was investigated in two asymptotic limits. Upon complete fusion ($D = 0$), the system degenerates into a single spherical QD of radius a, and the calculated energy values perfectly match the spectrum of an isolated QD. In the opposite case ($D >> 2a$), the geometric overlap and the tunneling probability vanish. The energy splitting ΔE tends to zero, and the E_0 and E_1 levels merge into a doubly degenerate state with an energy equal to that of an isolated QD of radius a. Such a consistent asymptotic transition to the known solutions confirms the mathematical rigor of the constructed Hamiltonian and the derived Fourier transform of the

To gain a deeper understanding of the physical mechanisms governing the evolution of the energy spectrum, the spatial distribution of the wave functions was investigated. Figure 3 presents the cross-sections of the electron probability density $|\psi(x, 0, z)|^2$ in the $y = 0$ plane for the five lowest energy states. The calculations were performed for a fixed constituent sphere radius of $a = 5$ nm at various inter-center distances D.

In the weak tunneling coupling regime, where the QDs are physically separated by the host matrix potential barrier ($D = 15$ nm, bottom row, Fig. 3.), the wave functions clearly exhibit a molecular-like character typical of quantum molecule systems. The ground (first column, Fig. 3) and first excited (second column, Fig. 3) states are formed as symmetric and antisymmetric linear combinations of the 1s-like states of the isolated QDs. In both cases, the electron density remains strongly localized within the nanospheres, and the probability of finding an electron in the space between them is extremely low. The third, fourth, and fifth columns correspond to higher spatial harmonics (analogs of p-states), which also demonstrate strict localization within their respective spherical regions.

Decreasing the distance to the point of physical contact ($D = 10$ nm) and the subsequent fusion of the nanocrystals ($D = 8$ nm) leads to the formation of a single dumbbell-shaped quantum molecule with a pronounced

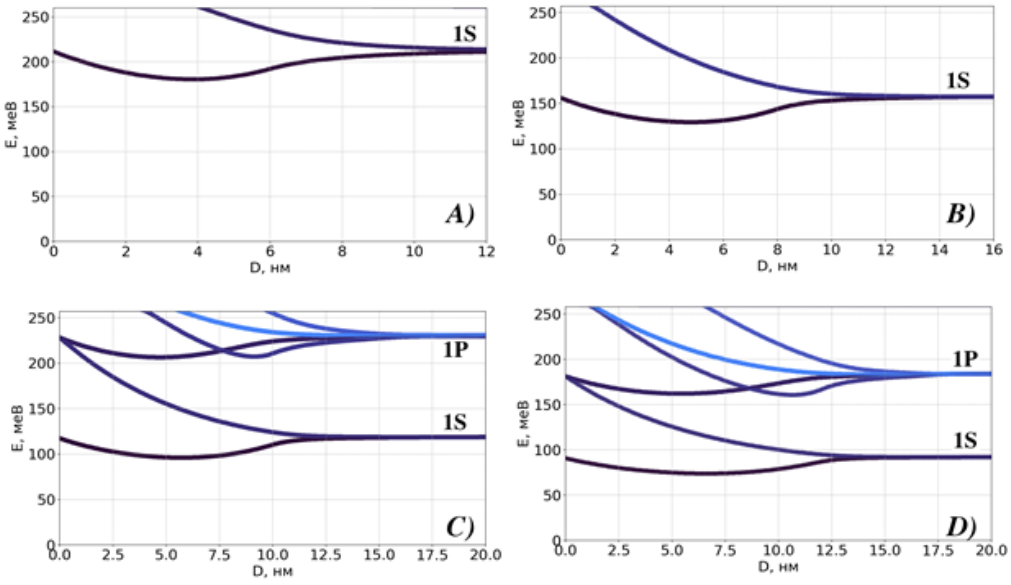

Fig. 2. Dependence of the lowest electron energy levels on the inter-center distance D in the fused $GaAs/Al_{0.3}Ga_{0.7}As$ QD. The calculated curves correspond to different fixed values of the sphere's radius: A – $a = 3$ nm, B – $a = 4$ nm, C – $a = 5$ nm, and D – $a = 6$ nm.

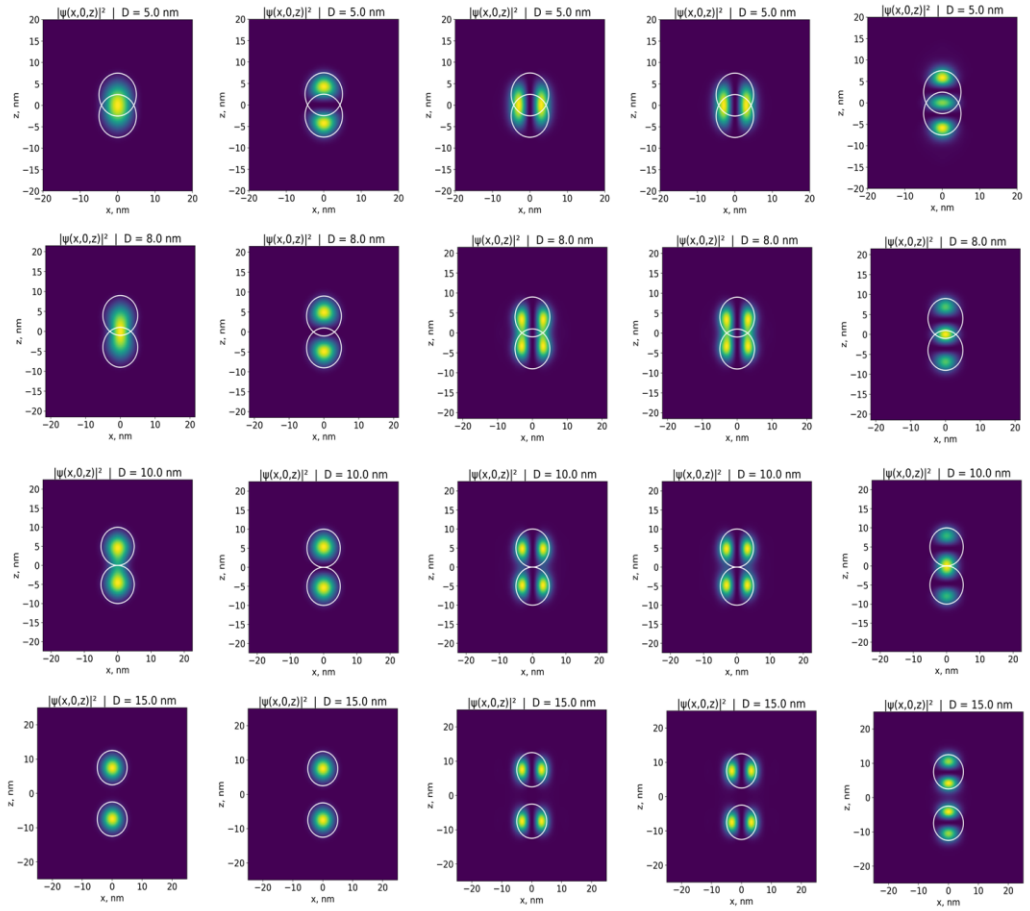

Fig. 3. Spatial distribution of the electron probability density for the lowest states, illustrating the transition from fused QDs of complex geometry to tunnel-coupled ones. The results are shown for constituent spheres of radius a = 5 nm at various inter-center distances D: ranging from a single, strongly coupled dumbbell-shaped nanostructure at D = 5 nm (first row) to the weak tunneling regime at D = 15 nm (last row). From left to right, the columns correspond to the increasing order of the states (e.g., ground state, first excited state, etc.).

"neck". In this regime, the spatial distribution undergoes fundamental changes. The symmetric ground state with energy E_0 becomes strongly delocalized. The barrier vanishes, and a significant portion of the electron density flows into the intersection region of the spheres (the neck), which is physically equivalent to the formation of a strong covalent bond. In contrast, the first excited state, being antisymmetric, possesses a strict nodal plane at z = 0 (exactly at the center of the neck), where the probability of finding an electron is zero. It is precisely this spatial overlap of the wave functions in the geometric fusion region that causes the exponential increase in the energy splitting observed in the energy spectra.

In the limit of strong fusion (D = 5 nm, top row, Fig. 3), when the center of one sphere lies on the surface of the other, the system completely loses its two-dot individuality and behaves as a single elongated QD of complex shape. The wave function of the ground state takes the form of an almost perfect ellipsoid centered at the center of mass of the overall structure. The higher excited states (columns 3–5, Fig. 3) evolve in their symmetry from a set of isolated p-like orbitals to the corresponding longitudinal and transverse spatial harmonics of a single continuous nanostructure.

Conclusions

In this work, we theoretically investigated the electron energy spectrum and wave functions of fused QDs. We successfully applied the plane-wave expansion method by deriving an exact analytical Fourier transform of the complex shape function using cylindrical Bessel functions, enabling fast Hamiltonian diagonalization without 3D grids. For the GaAs/AlGaAs system, we demonstrated that the state energies decrease as the inter-center distance D is reduced. In the strong overlap regime ($D < 2a$), quantum-mechanical hybridization causes the energy levels to split into symmetric and antisymmetric states, with the energy splitting increasing exponentially. The spatial probability density clearly illustrates the transition from a weak tunneling regime to a strongly coupled dumbbell-shaped nanostructure. Finally, the model's validity was confirmed by its exact convergence to the known solutions for isolated spherical quantum dots in the asymptotic limits, when D = 0 and D >> 2a.

Leshko Roman **–** PhD in Physics and Mathematics, Associate Professor of the Department of Physics and Information Systems;
Leshko Olha **–** PhD in Physics and Mathematics, Junior Research Associate;
Bilynskyi Ihor – Sc.D. in Physics and Mathematics, Professor of the Department of Physics;
Melnyk Yaroslav – Phd-student of the Department of Physics;
Ocheretyanyi Andriy – Phd-student of the Department of Physics;
Chekin Oleksandr – Phd-student of the Department of Physics;
Kvyk Marko – Phd-student of the Department of Physics.

[1] F. Pelayo García de Arquer et al., *Semiconductor quantum dots: Technological progress and future challenges*, Science, 373, eaaz8541 (2021); https://doi.org/10.1126/science.aaz8541.
[2] S. Koley, J. Cui, Y. E. Panfil, and U. Banin, *Coupled Colloidal Quantum Dot Molecules*, Acc. Chem. Res, 54. 1178 (2021); https://doi.org/10.1021/acs.accounts.0c00691.
[3] J. Cui, Y.E. Panfil, S. Koley, et al., *Colloidal quantum dot molecules manifesting quantum coupling at room temperature*, Nature Communication, 10, 5401 (2019); https://doi.org/10.1038/s41467-019-13349-1.
[4] Eunjoo Jang, Hyosook Jang, *Review: Quantum Dot Light-Emitting Diodes,* Chemical Reviews, 123 (8), 4663 (2023); https://doi.org/10.1021/acs.chemrev.2c00695.
[5] P. Senellart, G. Solomon & A. White, *High-performance semiconductor quantum-dot single-photon sources*, Nature Nanotechnology, 12, 1026 (2017); https://doi.org/10.1038/nnano.2017.218.
[6] Stefania Castelletto, Alberto Boretti, *Luminescence solar concentrators: A technology update*, Nano Energy, 109, 108269 (2023); https://doi.org/10.1016/j.nanoen.2023.108269.
[7] I. Medintz, H. Uyeda, E. Goldman, et al., *Quantum dot bioconjugates for imaging, labelling and sensing*, Nature Mater, 4, 435 (2005); https://doi.org/10.1038/nmat1390.
[8] Hancong Li, Qiming Peng, Xiulai Xu, Jianpu Wang, *Quantum dots for optoelectronics*, Advanced Photonics, 5(6), 060503 (2023); https://doi.org/10.1117/1.AP.5.6.060503.
[9] Liberato Manna, *The Bright and Enlightening Science of Quantum Dots*, Nano Letters, 23. 9673 (2023); https://doi.org/10.1021/acs.nanolett.3c03904.
[10] G.A. Mantashian, P. A. Mantashyan, D. B. Hayrapetyan, *Modeling of Quantum Dots with the Finite Element Method,* Computation, 11. 5 (2023); https://doi.org/10.3390/computation11010005.
[11] J. Ahmed, S. Sharma, K. V. Ramanujachary, S. E. Lofland, A. K. Ganguli, *Microemulsion-mediated synthesis of cobalt (pure fcc and hexagonal phases) and cobalt-nickel alloy nanoparticles*, Journal of Colloid and Interface Science, 336(15), 814 (2009); https://doi.org/10.1016/j.jcis.2009.04.062.
[12] J.S. Hu, Y.G. Guo, H.P. Liang, L.J. Wan, L. Jiang, *Three-dimensional selforganization of supramolecular self-assembled porphyrin hollow hexagonal nanoprisms,* Journal of the American Chemical Society, 127(48), 17090 (2005); https://doi.org/10.1021/ja0553912.
[13] M. Jitianu, D. V. Goia, *Zinc oxide colloids with controlled size, shape, and structure*, Journal of Colloid and Interface Science, 309(1), 78 (2007); https://doi.org/10.1016/j.jcis.2006.12.020.
[14] X. Qu, L. Omar, T. B. H. Le, L. Tetley, K. Bolton, K. W. Chooi, W. Wang, I. F. Uchegbu, *Polymeric Amphiphile Branching Leads to Rare Nanodisc Shaped Planar Self-Assemblies*, Langmuir, 24(18), 9997 (2008); https://doi.org/10.1021/la8007848.
[15] Vincent Notot, Willem Walravens, Maxime Berthe, Nemanja Peric, Ahmed Addad, Xavier Wallart, Christophe Delerue, Zeger Hens, Bruno Grandidier, and Louis Biadala, *Quantum Dot Acceptors in Two-Dimensional Epitaxially Fused PbSe Quantum Dot Superlattices,* ACS Nano, 16, 3081 (2022); https://doi.org/10.1021/acsnano.1c10596.
[16] A. Abelson, C. Qian, T. Salk, et al., *Collective topo-epitaxy in the self-assembly of a 3D quantum dot superlattice*, Nature Materials, 19, 49 (2020); https://doi.org/10.1038/s41563-019-0485-2.
[17] Philipp Schapotschnikow, Marijn A. van Huis, Henny W. Zandbergen, Daniël Vanmaekelbergh, and Thijs J. H. Vlugt, *Morphological Transformations and Fusion of PbSe Nanocrystals Studied Using Atomistic Simulations,* Nano Letters, 10, 3966 (2010); https://doi.org/10.1021/nl101793b.
[18] Luis Tortajada, Lucas V. Besteiro, Murilo L. Tiago, L. J. Gallego, James R. Chelikowsky, and M. M. G. Alemany, *Multidimensional nanoscale materials from fused quantum dots*, Phys. Rev. B, 84, 205326 (2011). https://doi.org/10.1103/PhysRevB.84.205326.
[19] Tewodros Adaro Gatissa, Teshome Senbeta Debela, Belayneh Mesfin Ali, *Effect of cubic and spherical quantum dot size and size dispersion on the performance of quantum dot solar cells*, AIP Advances, 14, 015236 (2024); https://doi.org/10.1063/5.0184745.
[20] Wei Li, Thomas M. Sabel. *Reinvestigation of quantum dot symmetry: the symmetric group of the 8-band k·p theory Hamiltonian,* Journal of Nanoparticle Research, 21, 16 (2019); https://doi.org/10.1007/s11051-018-4448-3.
[21] F.A. Donado, F.G. Almanza, C.F. Viña, and al., *Impact of Nonresonant Intense Laser and Electric Fields on a Low-Dimensional CdTe/CdSe Type-II Cone*, Nanomaterials, 15, 1208 (2025); https://doi.org/10.3390/nano15151208.

[22] V. Hols'kyi, R. Leshko, *The influence of deformations on single electron states in a molecule formed from three quantum dots of the heterosystem InAs/GaAs*, Physics and Chemistry of Solid State, 23(4), 686 (2022); https://doi.org/10.15330/pcss.23.4.686-692.
[23] R. Ya. Leshko, I. V. Bilynskyi, O. V. Leshko, M. A. Slusarenko, *Electron energy spectrum of the non-concentric spherical core-shell quantum dot*, Micro and Nanostructures, 181, 207615 (2023); https://doi.org/10.1016/j.micrna.2023.207615.
[24] R. Ya. Leshko, O. V. Leshko, I. V. Bilynskyi, M. V. Kvyk, Ya. Yu. Melnyk, A.O. Ocheretyanyi, M. Yu. Popov, *Electron and hole energy spectra in a non-concentric spherical core-shell quantum dot under a magnetic field*, Physics Letters A, 562, 130996 (2025); https://doi.org/10.1016/j.physleta.2025.130996.
[25] I. Bilynskyi, R. Leshko, O. Leshko, H. Terletska, R. Pazuyk, & K. Voitovych, *Impurity states in non-concentric spherical core-shell quantum dot*, Physics and Chemistry of Solid State, 25(1), 98 (2024); https://doi.org/10.15330/pcss.25.1.98-103.
[26] Shu-Shen Li and Jian-Bai Xia, *Binding energy of a hydrogenic donor impurity in a rectangular parallelepiped-shaped quantum dot: Quantum confinement and Stark effects*, Journal of Applied Physics, 101, 093716 (2007); http://dx.doi.org/10.1063/1.2734097.
[27] S. Sanguinetti, K. Watanabe, T. Tateno, M. Gurioli, P. Werner, M. Wakaki, N. Koguchi, *Modified droplet epitaxy GaAs/AlGaAs quantum dots grown on a variable thickness wetting layer,* Journal of Crystal Growth, 253(1–4), 71 (2003); https://doi.org/10.1016/S0022-0248(03)01016-9.
[28] S. Bietti, F.B. Basset, A. Tuktamyshev, et al, *High–temperature droplet epitaxy of symmetric GaAs/AlGaAs quantum dots*, Scientific Reports, 10, 6532 (2020); https://doi.org/10.1038/s41598-020-62248-9.
[29] P. Harrison and A. Valavanis, Quantum Wells, Wires and Dots: Theoretical and Computational Physics of Semiconductor Nanostructures, 4th ed. (John Wiley & Sons, Chichester, 2016).

Р.Я. Лешко[1], О.В. Лешко[1], І.В. Білинський[1,2], Я.Ю. Мельник[2], А.О. Очеретяний[2], О.І. Чекін[2], М.В. Квик[2]

Енергетичний спектр електрона в розділених та злитих сферичних квантових точках

[1]*Кафедра фізики та інформаційних систем, Дрогобицький державний педагогічний університет імені Івана Франка, м. Дрогобич, Україна, leshkoroman@dspu.edu.ua;*
[2]*Кафедра фізики та методики її викладання, Криворізький державний педагогічний університет, м. Кривий Ріг, Україна*

Пропонується ефективний напіваналітичний підхід для моделювання електронних станів у злитих сферичних квантових точках, заснований на виведенні точного аналітичного перетворення Фур'є їх тривимірної функції форми за допомогою циліндричних функцій Бесселя. Цей математичний підхід дозволяє безпосередньо застосовувати метод розкладання за плоскими хвилями до систем зі складною, несепарабельною геометрією. Для гетероструктури GaAs/AlGaAs показано, що зменшення міжцентрової відстані D спричиняє монотонне зниження енергій електрона, тоді як у режимі сильного геометричного перекриття ($D < 2a$) квантово-механічна гібридизація розщеплює рівні енергії на симетричні та антисиметричні стани. Графіки просторового розподілу густини ймовірності наочно демонструють перехід від режиму слабкого тунелювання (молекулярноподібні стани) до сильно зв'язаної наноструктури у формі гантелі.

Ключові слова: злиті та зв'язані квантові точки, енергетичний спектр електрона, гібридизація хвильових функцій.